Applied Catalysis B: Environmental 147 (2014) 888–896

Contents lists available at ScienceDirect

Applied Catalysis B: Environmental

journal homepage: www.elsevier.com/locate/apcatb

Hierarchical sulfonated graphene oxide–TiO_2 composites for highly efficient hydrogen production with a wide pH range

Peng Gao, Darren Delai Sun *

School of Civil and Environmental Engineering, Nanyang Technological University, 50 Nanyang Avenue, Singapore 639798, Singapore

ARTICLE INFO

Article history:
Received 19 July 2013
Received in revised form 11 October 2013
Accepted 12 October 2013
Available online 18 October 2013

Keywords:
Hierarchical composites
Hydrogen
pH
Sulfonation
Titanates

ABSTRACT

Synthesizing highly efficient photocatalyst for hydrogen production still remains a great challenge, especially generating hydrogen from water with a wide pH range. In this work, for the first time, the hierarchical sulfonated graphene oxide (SG)–TiO_2 composites were successfully synthesized by ultrasonic mixing SG sheets and TiO_2 spheres. SG–TiO_2 composites exhibit high hydrogen production efficiency with a wide pH range (from pH = 3 to pH = 11). Under neutral pH (pH = 7), SG–TiO_2-2 composite with the optimal amount of 2% SG sheets achieves the highest hydrogen evolution rate (ca. 260 μmol/h), which is more than 11 times higher than that of pure TiO_2 and P25. The high hydrogen evolution rate can be owed to the promising properties of SG–TiO_2 composites, including large surface area, efficient light absorption ability and high charge separation efficiency. More interestingly, SG–TiO_2 composites can perform excellent hydrogen production activity under different pH conditions, even under alkaline condition, where the hydrogen production efficiency of GO–TiO_2 composites usually decreased dramatically under such condition. This particular phenomenon can be attributed to the tight coordination between the SG sheets and TiO_2 spheres, which prevents the damage of SG–TiO_2 composites in the alkaline solution. Consequently, these novel SG–TiO_2 composites can be widely applied in the practical clean energy production field.

1. Introduction

Fossil fuels as the traditional main energy source have been over exploited since the industrial revolution. The excessive consumption of fossil fuels leading to global warming have impelled the researchers from all over the world to look for other renewable clean energy [1]. Hydrogen as a clean energy has attracted great interest as a replacement for the traditional energy sources in view of its high heat conversion efficiency and zero carbon emission [2,3]. Hence, it is a promising alternative to solve the current energy crisis and environmental problems. Semiconductor-based photocatalytic production of hydrogen has been the hot subject of tremendous research, since the first discovery of photocatalytic water splitting by n-type TiO_2 photo-electrodes in 1972 [4].

Till now, TiO_2 has been an intensively investigated photocatalyst to produce hydrogen among a diversity of semiconductors because of its outstanding properties, including chemical stability, non-toxicity and abundant in resources [5]. However, two main limitations of TiO_2, including wide band gap (3.2 eV for anatase and 3.0 eV for rutile) and rapid charge recombination rate, significantly restrict the performance of pure TiO_2 [6,7]. Therefore, to date, many approaches have been invented in order to overcome these drawbacks, including metal or nonmetal doping [8–12], coupling with other semiconductors [13–15] and combination with carbon based materials (carbon nanotubes, graphene and graphene oxide (GO)) [16–18]. In particular, graphene/graphene derivatives (GO or other forms of functionalized graphene) based TiO_2 composites have attracted an intensive amount of research interests from both energy generation and environmental remediation fields [19–26]. This is because graphene and its derivatives acquire promising properties, such as large specific surface area (theoretically 2600 m^2/g), fast charge transfer rate, high flexibility and chemical stability [27,28]. In view of these, the light absorption ability of graphene/GO based TiO_2 composites can be enhanced due to the existence of graphene/GO sheets [18]. In addition, graphene/GO sheets can facilitate charge transfer and reduce recombination rate of electron-hole pairs, further improving the photocatalytic efficiency [17,29].

To date, there are a few graphene/GO–TiO_2 composites have been prepared and applied in the phtotocatalytic hydrogen production field [17,18,30–33]. Zhang et al. synthesized graphene/TiO_2 nanocomposites through a sol–gel method using tetrabutyl titanate (TBT) and GO as precursors [30]. They concluded that graphene/TiO_2 composites with 5% graphene sheets exhibit the highest water splitting efficiency, which is much higher than that of P25. Choi and co-workers prepared GO–TiO_2 composites by

* Corresponding author. Tel.: +6567906273; fax: +65 6791 0676.
E-mail address: ddsun@ntu.edu.sg (D.D. Sun).

0926-3373/$ – see front matter © 2013 Elsevier B.V. All rights reserved.
http://dx.doi.org/10.1016/j.apcatb.2013.10.025

self-assembling P25 nanoparticles on GO sheets and investigated the effects of size of GO sheets on the hydrogen production activity [31]. They reported that the GO–TiO_2 composites with small GO sheets could obtain better performance than that with large GO sheets because of enhanced interfacial charge transfer. Very recently, Yu's group investigated the synergetic effect of MoS_2 and graphene sheets on the hydrogen production activity of TiO_2 nanoparticles [17]. In their work, it has been demonstrated that TiO_2/MoS_2/graphene composite can achieve a high hydrogen evolution rate even without noble metal (Pt). However, the hydrogen production activities of graphene/GO–TiO_2 composites in these reported results were only investigated under neutral pH. According to our previous experiences, graphene/GO–TiO_2 composites would be destroyed under alkaline condition due to the damage of interaction between graphene/GO sheets and TiO_2 [34,35]. This significantly hinders the application of graphene/GO–TiO_2 composites in the basic condition. Hence, it is urgent but challenging to synthesize functionalized graphene/GO–TiO_2 composites, which can tolerate different environment and can acquire efficient hydrogen production activity within a wide pH range.

In this study, for the first time, we report the highly efficient hydrogen production activity of sulfonated graphene oxide (SG)–TiO_2 composites under a wide pH range (from pH = 3 to pH = 11). SG–TiO_2 composites were prepared by a step-wise method. Firstly, SG sheets were synthesized by introducing sulfonic acid groups ($-SO_3H$) into GO sheets through sulfonation reaction. Then, SG–TiO_2 composites were prepared *via* uniformly mixing SG sheets and TiO_2 spheres on micro-scale under ultrasonication. The results show that SG–TiO_2 composites exhibit significantly higher hydrogen evolution rate than P25 and pure TiO_2 spheres under neutral pH. This is because of the outstanding properties of SG–TiO_2 composites, including large specific surface area, enhanced light absorption and efficient charge separation. Particularly, SG–TiO_2 composites can achieve a high hydrogen evolution rate under alkaline condition, while the hydrogen generation rate of GO–TiO_2 was decreased significantly in basic solution. This can be attributed to the strong interaction between SG sheets and TiO_2 spheres, endowing it a stable and efficient photocatalyst within a wide pH range. Hence, these novel SG–TiO_2 composites can be promising candidates for clean energy production under different environmental condition.

2. Experimental methods

2.1. Materials

Tetrabutyl titanate (TBT), sodium nitrate ($NaNO_3$, 99%), potassium permanganate ($KMnO_4$, 99%), hydrogen peroxide (H_2O_2, 35%), concentrated sulfuric acid (H_2SO_4, 98%), sodium 2-chloroethanesulfonate hydrate ($ClCH_2CH_2SO_3H$), hydrochloric acid (HCl, 37%), sodium hydroxide (NaOH) were obtained from Sigma-Aldrich. Dimethyl formamide (DMF) and isopropyl alcohol (IPA) were purchased from Merck Ltd. In addition, natural graphite (SP1) was obtained from Bay Carbon Company (USA). All chemicals were used without further purification. Furthermore, deionized (DI) water was produced from Millipore Milli-Q water purification system.

2.2. Synthesis of GO and SG

GO sheets were prepared according to the modification of Hummer's method [36], and the procedure was reported in the previous work [37–39]. SG sheets were prepared by a sulfonation reaction [40]. Typically, 200 mg of GO, 3 g of $ClCH_2CH_2SO_3H$ and 1.6 g of NaOH were added into 500 mL of DI water. The mixture was put under ultrasonication condition for 3 h and then 2 mL of HNO_3 was added into the mixture. Finally, the mixture was washed with ethanol for three times and put into vacuum drier for 2 days.

2.3. Synthesis of hierarchical TiO_2 sphere

Hierarchical TiO_2 spheres were prepared according to the slight modification of previous reported method [41]. In a typical process, 1 mL of TBT was added the mixture of 15 mL of DMF and 15 mL of IPA drop by drop. Then, the mixture was transferred to a Teflon-lined stainless-steel autoclave (volume: 45 mL), which was then heated to 200 °C and kept for 20 h. The product was collected by centrifugation after the autoclave cooled to room temperature and followed by ethanol washing. Finally, the material was dried at 60 °C for 24 h and calcined at 450 °C for 2 h with a ramping rate of 5 °C/min.

2.4. Synthesis of SG–TiO_2 composites

A number of SG–TiO_2 composites were prepared by adjusting the mass ratio of SG to TiO_2. Various amount of as-synthesized SG powder (0.5 mg, 1 mg, 2 mg, 3 mg and 5 mg) was well dissolved in 100 mL of DI water. Then, 100 mg of as-prepared hierarchical TiO_2 sphere was added to the above SG solution, respectively. The mixture was put in the ultrasonic bath for 2 h. Finally, the mixture was centrifuged and put into vacuum drier for further usage. The prepared samples were indicated as SG–TiO_2-0.5, SG–TiO_2-1, SG–TiO_2-2, SG–TiO_2-3 and SG–TiO_2-5 according to the mass ratio of SG to TiO_2.

2.5. Characterization

Surface topography of GO and SG sheets was characterized by atomic force microscopy (AFM, PSIA XE-150). The morphologies of hierarchical TiO_2 sphere and SG–TiO_2 composites were evaluated by field emission scanning electron microscopy (FESEM, JSM-7600F). Transmission electron microscopy (TEM) and high-resolution TEM (HRTEM) images of TiO_2 and SG–TiO_2 were acquired using a JEOL 2010-H microscope (TEM) operating at 200 kV. The structure and crystal phase of GO, SG, TiO_2 and SG–TiO_2 were examined by X-ray diffraction (XRD, Shimadzu XRD-6000) with monochromated high-intensity Cu *K*α radiation (λ = 1.5418 Å) operated at 40 kV and 30 mA. FTIR spectra were recorded on a Perkin Elmer GX FT-IR system by using compressed KBr disc technique. In addition, X-ray photoelectron spectroscopy (XPS) measurements were done by using a Kratos Axis Ultra Spectrometer with a monochromic Al *K*α source at 1486.7 eV, with a voltage of 15 kV and an emission current of 10 mA. The binding energy (BE) values were calibrated by using carbonaceous C 1s line (284.8 eV) as a reference. Photoluminescence (PL) spectra were measured on the spectrofluorophotometer (Shimadzu RF-5301). Furthermore, the Brunauer–Emmet–Teller (BET) specific surface area of TiO_2 and SG–TiO_2 was determined at liquid nitrogen temperature (77 K) using the Micromeritics ASAP 2040 system. The pore size distribution is calculated from the desorption branch of the isotherm according to the BJH model.

2.6. Photocatalytic hydrogen production under different pH

The photocatalytic hydrogen production reaction was performed in a three-necked Pyrex flask (volume: 100 mL) with the three openings of the flask were sealed by silicone rubber. 2 low-pressure UVP Pen-Ray mercury lamps (254 nm, 5.4 mW cm^{-2}, USA) were used as UV light source and put 2 cm beside the flask. To maintain a constant reactor temperature of 25 °C, the flask was cooled by water under the bottom. 50 mg of powdered photocatalyst was suspended in 10 vol% methanol water mixture. A magnetic stirrer was

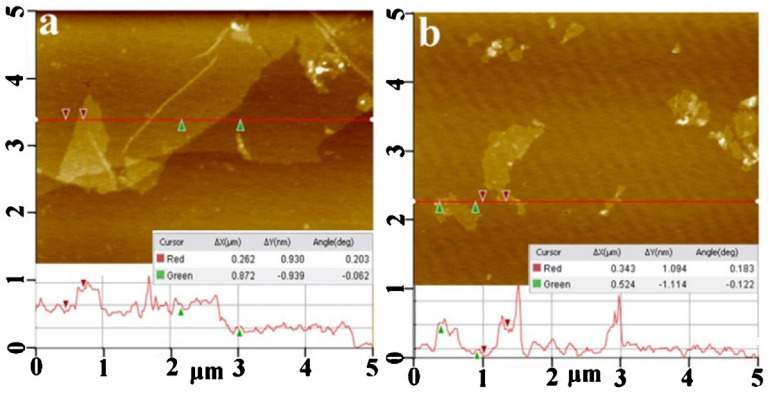

Fig. 1. AFM images of (a) GO and (b) SG sheets (inset: two-line scans).

placed at the bottom of the reactor to ensure homogeneity of the suspension during reaction. Prior to irradiation, the photocatalyst suspension was de-aerated thoroughly for 30 min by nitrogen gas purging. Gas produced *via* the photocatalytic reaction was analyzed using an off-line TCD-type gas chromatography (Agilent 7890A, HP-PLOT MoleSieve/5A). The pH of the solution was adjusted with dilute NaOH and HCl solution.

3. Results and discussion

3.1. Morphology and structure properties of SG–TiO_2 composites

Surface topography of GO sheets and SG sheets was well characterized by AFM, as presented in Fig. 1. Fig. 1a shows the single layer and some overlap of GO sheets with the size around several micrometers. In addition, as seen in the inset of Fig. 1a, the thickness of GO sheet is about 0.93 nm measured through two line scans, which is coordinated well with the reported thickness of single layer GO [31,37]. After sulfonation reaction, the size of GO sheets was significantly reduced. Fig. 1b shows that the size of SG sheets is around several hundred nanometers and the thickness is about 1.1 nm which is a little larger than that of GO sheets. The increase of the thickness can be attributed to the introduction of sulfonic acid groups. In addition, the reduction in the size of the SG sheets is a key point in preparing SG–TiO_2 composites. If the SG sheets are too large, they will fully wrap the TiO_2 sphere, which reduces the penetration of light and the activity of TiO_2.

Fig. 2a and b are the FESEM images of unannealed TiO_2 spheres. Fig. 2a shows that the size of these hierarchical TiO_2 spheres is uniform with the diameter of around 500 nm. In addition, a closer observation indicates that these TiO_2 spheres are actually assembled by thin two-dimensional (2D) sheets with the thickness of ca. 10 nm, as seen in Fig. 2b. After heat treatment in air at 450 °C for 2 h, the morphology of TiO_2 spheres has a remarkable change, as exhibited in Fig. 2c and d. The size of the annealed TiO_2 spheres has no obvious shrinkage, while the void-free 2D sheets of unannealed sphere change to the porous structures which are in fact constructed by crystallized TiO_2 nanoparticles. The formation of pores is because of the evaporation of the organic precursor. TEM images of unannealed and annealed TiO_2 spheres (Fig. 2e, f and Fig. S1) further verified that the unannealed TiO_2 spheres are constructed by ultra-thin 2D sheets, while annealed TiO_2 spheres are composed of numerous nanoparticles. Fig. 2g is the HRTEM image taken from one nanoparticle of annealed TiO_2 sphere. The distinctive lattice fringe of ca. 0.35 nm can be assigned to the (1 0 1) crystal plane of the anatase TiO_2, indicating that annealed TiO_2 spheres are highly crystallized. The good crystalinity of the TiO_2 spheres can enhance the charge transfer and photocatalytic activity [42,43]. Fig. 2h is the SAED pattern of the annealed TiO_2 sphere and the diffuse ring pattern indicates that the TiO_2 spheres are polycrystalline structure.

The hierarchical SG–TiO_2 composites were synthesized by ultrasonic mixing SG sheets with TiO_2 spheres, as schematically illustrated in Fig. 3a. Firstly, TiO_2 spheres and SG sheets are well dispersed in water. Then, TiO_2 spheres are combined with SG sheets to form SG–TiO_2 composites under ultrasonication condition. Ultrasonication process can hinder the aggregation of SG sheets, which is a common problem for other synthetic methods, such as hydrothermal reaction. The single layer SG sheets can enhance the charge transfer rate between the TiO_2 spheres and SG sheets, compared with the aggregated SG sheets. The morphology of the SG–TiO_2 composites was well characterized by FESEM and TEM. Fig. 3b shows that the TiO_2 spheres were combined together by SG sheets and the sheets of TiO_2 spheres become blurry due to the existence of SG sheets, as compared with the images of pure TiO_2 spheres (Fig. 2c and d). TEM is a powerful technique to investigate the microstructure of graphene based composites. In Fig. 3c, one piece of SG sheets anchored on the edge of the TiO_2 sphere can be clearly observed. The characterized wrinkles of SG sheets and the highly crystallized anatase TiO_2 were indicated by white lines in the HRTEM image of Fig. 3d. According to the FESEM and TEM characterization, the hierarchical SG–TiO_2 composites were successfully synthesized *via* ultrasonic mixing.

The crystalline phases of GO, SG, TiO_2 and SG–TiO_2 composites were investigated by XRD. Fig. 4 shows the XRD patterns of as-synthesized samples, including GO, SG, TiO_2, SG–TiO_2-0.5, SG–TiO_2-1, SG–TiO_2-2, SG–TiO_2-3 and SG–TiO_2-5. In comparison with GO, the peak of SG shifts from 12° to 10.6°. This can be owed to the introduction of sulfonic acid groups into the layers of GO sheets, which increases the interlayer distance [35]. As shown in Fig. 4, TiO_2 spheres and all SG–TiO_2 composites show the remarkable diffraction peaks at 2θ of 25.3°, 38.2°, 48.1°, 53.5°, 55.6°, 62.7° and 75.0°, which can be indexed to the (1 0 1), (1 0 3), (2 0 0), (1 0 5), (2 1 1), (2 0 4) and (2 1 5) planes of the anatase TiO_2 (JCPDS card No. 21-1272).

The as-synthesized samples were also characterized by FTIR. Fig. 5a shows the FTIR spectra of GO, SG, TiO_2 and SG–TiO_2-2 composites, respectively. In Fig. 5a, the peaks of oxygen-containing functional groups of GO sheets are distinctly observed, including 1230 cm^{-1} (phenolic groups), 1389 cm^{-1} and 1726 cm^{-1} (carboxylic groups) [44,45]. The broad band ranging from 3200 cm^{-1} to 3600 cm^{-1} is characterized H–O–H bending band of adsorbed water [46]. In addition, the broad band between 400 cm^{-1} and 900 cm^{-1} of TiO_2 and SG–TiO_2-2 can be assigned to the Ti–O band. Fig. 5b is the high magnification FTIR spectra of GO and SG. It can be clearly identified that the peak intensity of SG at 1230 cm^{-1} is significantly reduced, while a small band at 1167 cm^{-1} (sulfonic acid groups) appears [47], compared with the spectrum of GO.

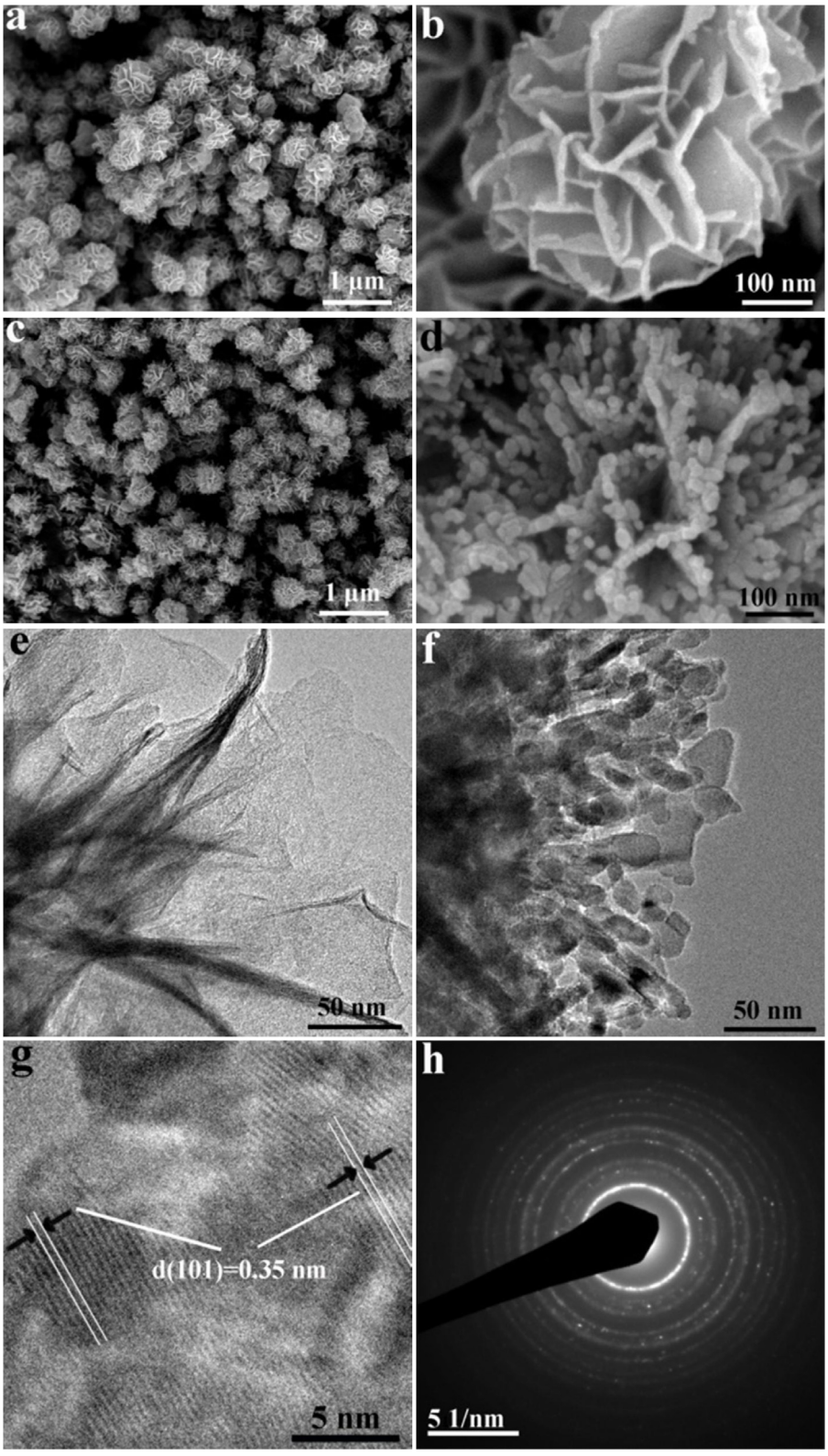

Fig. 2. (a) and (b) FESEM images of unannealed TiO_2 spheres; (c) and (d) FESEM images of annealed TiO_2 spheres; (e) TEM image of unannealed TiO_2 spheres; (f) TEM image of annealed TiO_2 spheres; (g) HRTEM image of annealed TiO_2 spheres; and (h) SAED pattern of annealed TiO_2 spheres.

GO, SG and SG–TiO_2-2 were further investigated by XPS spectra. Fig. 6a is the full-scan XPS spectra of GO, SG and SG–TiO_2-2, respectively. Only Ti, C, O and S elements can be found in SG–TiO_2-2 composites, indicating the high purity of as-synthesized SG–TiO_2. Fig. 6b shows the high resolution XPS spectra of S 2p from SG–TiO_2-2 composites. The peak of S 2p at ca. 167 eV confirms the successful combination of SG sheets with TiO_2 spheres. Fig. 6c is the high resolution spectra of C 1s from GO, SG and SG–TiO_2-2 from top to bottom. The intensity of C–O peak decreases remarkably from GO to SG because the C–O groups of GO have been partially

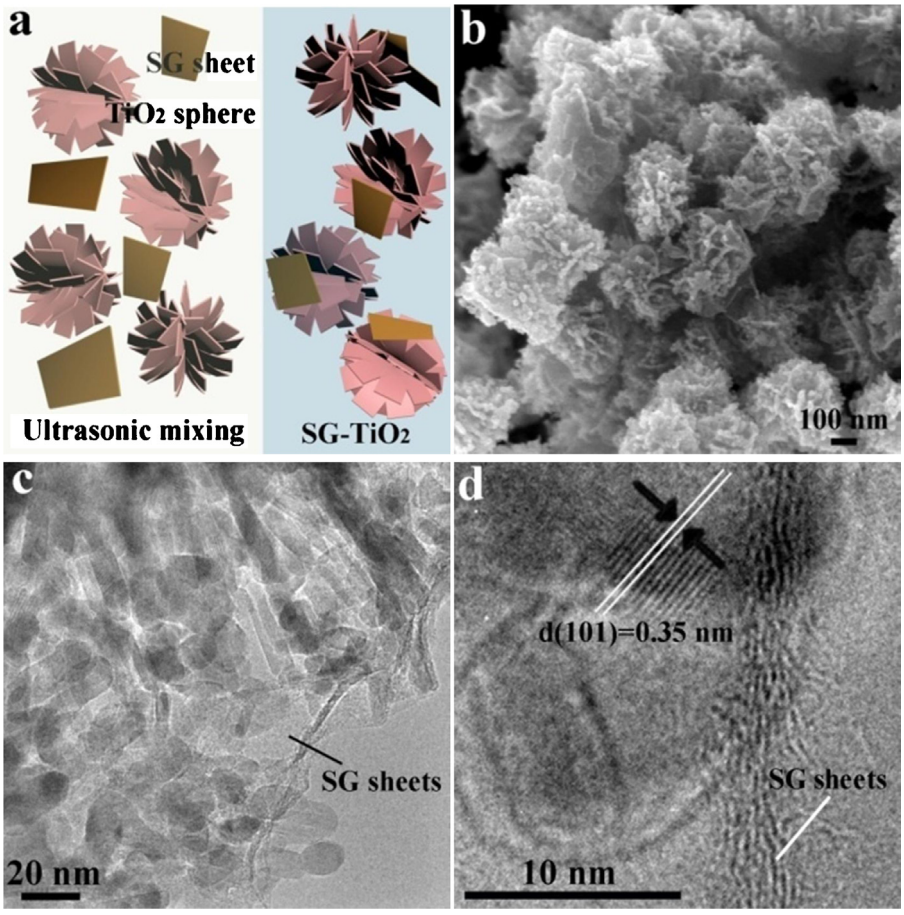

Fig. 3. (a) Schematic synthetic process of SG–TiO_2 composites; (b) FESEM images of SG–TiO_2 composites; (c) TEM image of SG–TiO_2 composites; and (d) HRTEM image of SG–TiO_2 composites.

converted into C–SO_3H groups in the sulfonation reaction. The high resolution XPS spectra of Ti 2p and O 2p from the SG–TiO_2-2 composites are shown in Fig. S2. Hence, the results of FTIR and XPS spectra demonstrate the successful preparation of SG sheets and SG–TiO_2 composites.

3.2. Photocatalytic hydrogen production activity under neutral pH

Fig. 7a and b shows the hydrogen production activities of a series of samples under UV light irradiation (254 nm). In Fig. 7a, it can be observed that pure TiO_2 spheres and commercial P25 nanoparticles exhibit limited hydrogen evolution capacity. Only around 41 μmol and 48 μmol of H_2 were produced by TiO_2 spheres and P25 within 2 h, respectively, because of rapid recombination of photo-generated electron–hole pairs. However, a great enhancement of hydrogen production activity can be achieved when the TiO_2 spheres are combined with SG sheets. About 193 μmol of H_2 was produced during 120 min when only 0.5 wt% of SG sheets were ultrasonic mixed with the TiO_2 spheres. The initial increase of SG sheets results in the increasing of hydrogen evolution activity, as shown in Fig. 7a. The optimal hydrogen production activity was obtained when 2 wt% of SG sheets were added, and ca. 530 μmol of H_2 was generated within 120 min, which is more than 11 times higher than that of pure TiO_2 spheres and P25. The hydrogen production activity was decreased when further increasing the amount of SG sheets. Only 137 μmol of H_2 was generated by SG–TiO_2-5, as displayed in Fig. 7a. This can be explained by the shielding effects of SG sheets because too much SG sheets will block the penetration of UV light and prevent the reaction between photo-generated holes and the sacrificial agents [48]. The hydrogen production activity was further investigated by comparing the effects of different synthetic methods including mechanical grinding and ultrasonic mixing. In addition, the influences of pristine GO sheets and functionalized SG sheets were also examined. Fig. 7b shows that more than 1000 μmol of H_2 is generated by the SG–TiO_2-2 composites (synthesized by ultrasonication), while only 210 μmol of H_2 is produced by the SG–TiO_2-2 composites (synthesized by mechanical mixing) within 4 h. The significant higher hydrogen evolution rate of ultrasonication prepared SG–TiO_2 composites than mechanical synthesized composites can be attributed to the better interfacial contact

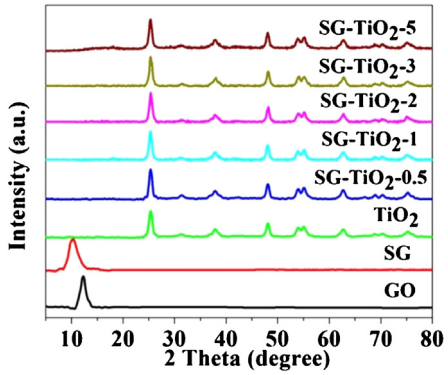

Fig. 4. XRD patterns of GO sheets, SG sheets and SG–TiO_2 composites.

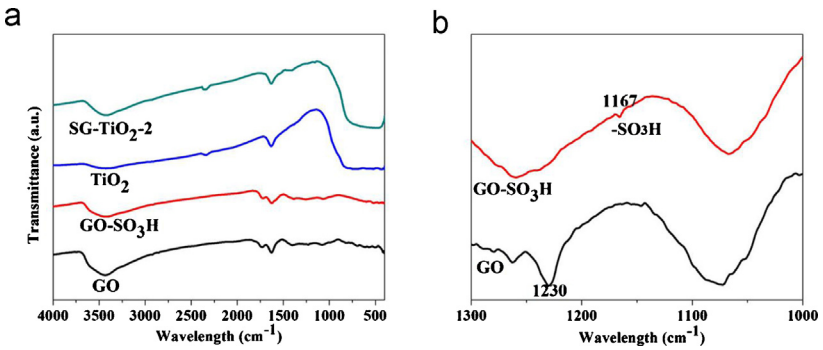

Fig. 5. (a) FTIR spectra of GO sheets, SG sheets, TiO_2 spheres and SG–TiO_2-2 composites; and (b) high magnification FTIR spectra).

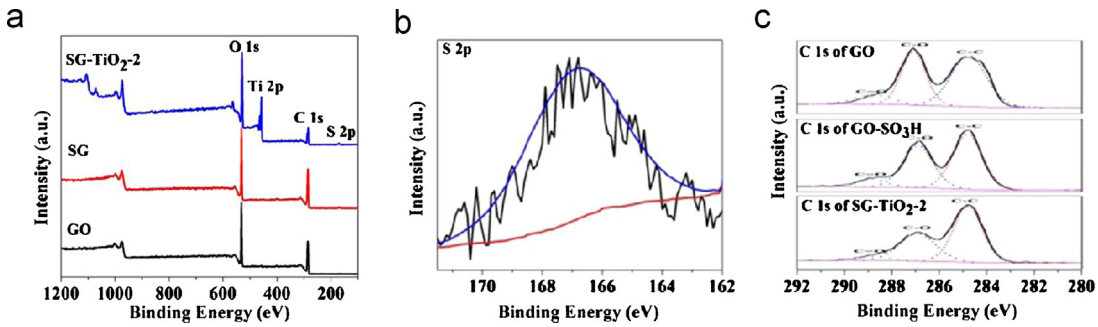

Fig. 6. (a) Full scan XPS spectra of GO sheets, SG sheets and SG–TiO_2-2 composites; (b) high resolution XPS spectra of S 2p from SG–TiO_2-2 composites; and (c) high resolution XPS spectra of C 1s from GO sheets, SG sheets and SG–TiO_2-2 composites (from top to bottom).

between SG sheets and TiO_2 spheres. As illustrated in Fig. 3a, the SG sheets can uniformly grafted on the TiO_2 spheres under ultrasonic mix, resulting in the enhanced interfacial adhesion, which can improve the efficiency of charge transfer [49]. GO–TiO_2 (2 wt% GO) shows comparable hydrogen evolution rate (245 μmol/h) with that of SG–TiO_2-2 (260 μmol/h), as presented in Fig. 7b. Table S1 shows that the hydrogen evolution rate of SG–TiO_2-2 is 260 μmol/h, which is higher than that of SG-P25 (200 μmol/h), SG–ZnO (156 μmol/h), and slightly lower than that of visible-light responsed SG-CdS (285 μmol/h). The apparent quantum efficiency of the photocatalyst can be calculated according to the reported equation [18]:

$$QE[\%] = \frac{\text{number of reached electrons}}{\text{number of incidemt photons}} \times 100$$

$$= \frac{\text{number of evolved H2 molecules} \times 2}{\text{number of incidemt photons}} \times 100$$

Hence, the quantum efficiencies of SG–TiO_2-2, SG-P25, SG–ZnO and SG-CdS are 2.30%, 1.77%, 1.38% and 2.52%, respectively.

3.3. Mechanism

Fig. 8 illustrates the reasons of the high photocatalytic hydrogen production rate of SG–TiO_2-2. Fig. 8a shows the N_2 adsorption–desorption isotherms of pure TiO_2 spheres and SG–TiO_2-2 composites, respectively. The BET surface area of SG–TiO_2-2 is 91.25 m^2/g, which is larger than that of TiO_2 spheres (75.36 m^2/g). In addition, the pore size distribution of TiO_2 ranges from 1 nm to 100 nm with two major peaks at around 3 nm and 30 nm, as shown in the inset of Fig. 8a. The pore size distribution of SG–TiO_2-2 is similar with that of TiO_2 except that the second peak shifts from 30 nm to 20 nm due to the deposition of SG sheets. The large surface area with mesoporous structure is beneficial for photocatalytic activity [43]. Fig. 8b shows the UV–vis absorption spectra of pure TiO_2 spheres and SG–TiO_2-2, respectively. In comparison with the spectrum of TiO_2, SG–TiO_2-2 composites acquire stronger absorption in the whole wavelength range (300 nm to 800 nm). The enhanced absorption of light is crucial to achieve excellent hydrogen production activity [18]. The UV–vis absorption

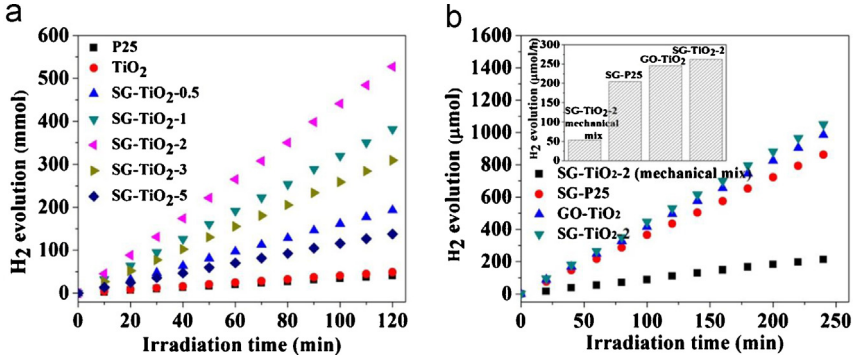

Fig. 7. (a) Hydrogen production activity of P25 nanoparticles, TiO_2 spheres and a series of SG–TiO_2 composites within 120 min; and (b) hydrogen production activity of SG–TiO_2-2 synthesized by mechanical grinding and ultrasonic mixing, SG-P25 (2 wt% of SG) and GO–TiO_2 (2 wt% of GO) (inset: average hydrogen evolution rate).

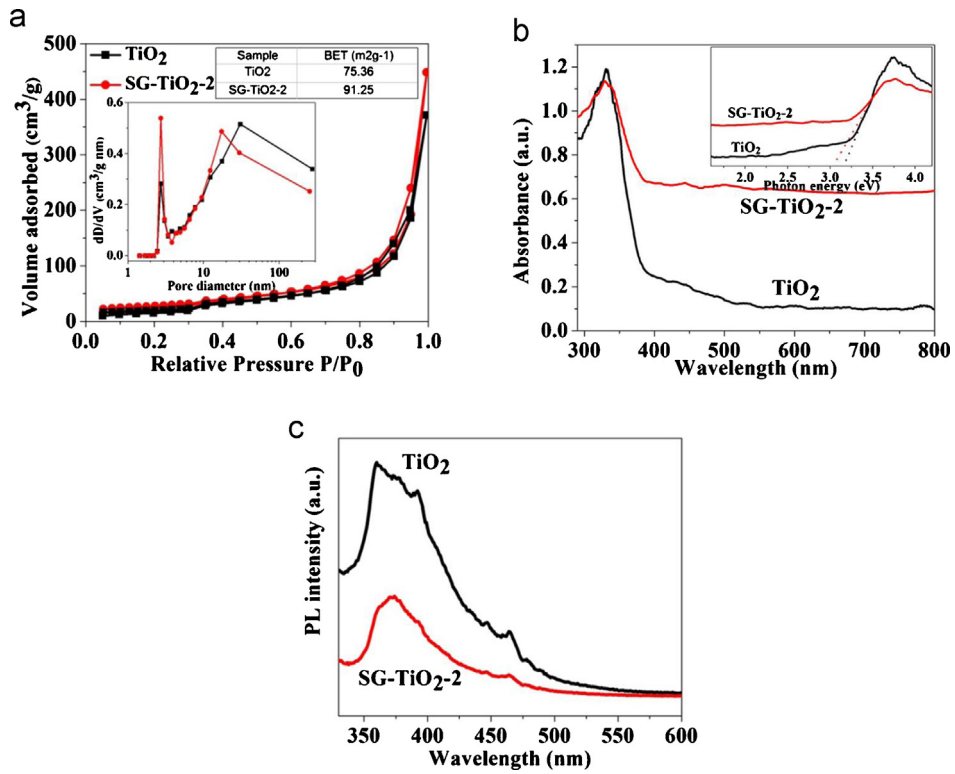

Fig. 8. (a) N_2 adsorption/desorption isotherm of TiO_2 spheres and SG–TiO_2-2 (inset: pore size distribution); (b) UV–vis spectra of TiO_2 spheres and SG–TiO_2-2 (inset: corresponding Kubelka–Munk transformed reflection spectra); and (c) PL spectra of TiO_2 spheres and SG–TiO_2-2.

spectra was further converted into the equivalent absorption coefficient (Eq. (1)) by the Kubelka–Munk function [50].

$$\alpha = \frac{(1-R)}{2R} \tag{1}$$

$\alpha$is optical absorption coefficient near the absorption edge for indirect interband transitions; R is the reflectance of the semiconductor, $R = 10^{-A}$, A is optical absorbance.

$$\alpha h\nu = C_1\left(h\nu - E_g\right)^2 \tag{2}$$

$$h\nu = \frac{1240}{\lambda} \tag{3}$$

C_1 is absorption constant for an indirect transition; $h\nu$ is photon energy; E_g is indirect band gap energy (eV); λ is wavelength (nm).

The straight line tangential to the vertical segment of the slope is extended to intersect the photon energy axis (X-axis) in obtaining E_g value of the samples, as shown in the inset of Fig. 8b. Hence, the band gaps of TiO_2 spheres and SG–TiO_2-2 composite are 3.16 eV and 3.02 eV, respectively. The band gap of SG–TiO_2-2 composite has a slightly red shift due to the presence of SG sheets. PL spectra of pure TiO_2 spheres and SG–TiO_2-2 were measured to investigate the charge separation process, as presented in Fig. 8c. Fig. 8c shows that the PL intensity of SG–TiO_2-2 is significantly lower than that of TiO_2, indicating that the charge recombination rate of SG–TiO_2-2 is much slower than that of TiO_2. This is because the photo-generated electrons can transfer from TiO_2 to SG sheets quickly. The mechanism of hydrogen production activity of SG–TiO_2 composites is schematically illustrated in Fig. 9. The electrons and holes of TiO_2 are generated firstly under light irradiation. Subsequently, the photo-generated electrons in the conduction band of TiO_2 can transfer to the SG sheets through the closely contacted interface. Finally, the photo-generated electrons react with protons to generate hydrogen, while the holes remaining in the valance band of TiO_2 oxidize the sacrificial methanol. Hence, the outstanding hydrogen generation activity of SG–TiO_2-2 can be attributed to (1) large specific surface area of mesoporous structure; (2) enhanced light scattering and absorption; and (3) anti-recombination of photo-generated electrons and holes.

3.4. Photocatalytic hydrogen production activity under acid and basic conditions

Considering the practical applicability of SG–TiO_2 composites in the engineering fields, the hydrogen production activity of SG–TiO_2 composites was investigated under different pH conditions. As shown in Fig. 10a, 653 μmol of H_2 was generated by SG–TiO_2-2 within 2 h under pH = 3 (acidic condition). In addition, the inset of Fig. 10a shows that the calculated hydrogen evolution rate of SG–TiO_2-2 is 326.5 μmol/h, which is higher than that of SG–TiO_2-2 (ca. 260 μmol/h) under pH = 7. The similar trends are also observed for the SG-P25 and GO–TiO_2. The increase of the

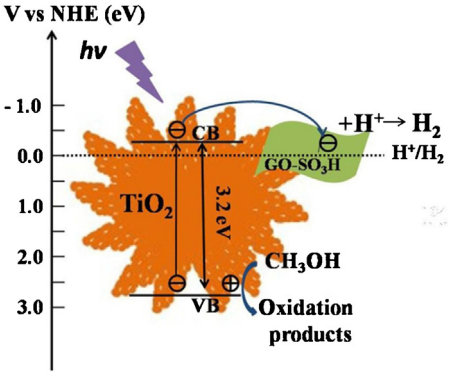

Fig. 9. Schematic mechanism of hydrogen production in SG–TiO_2 composites.

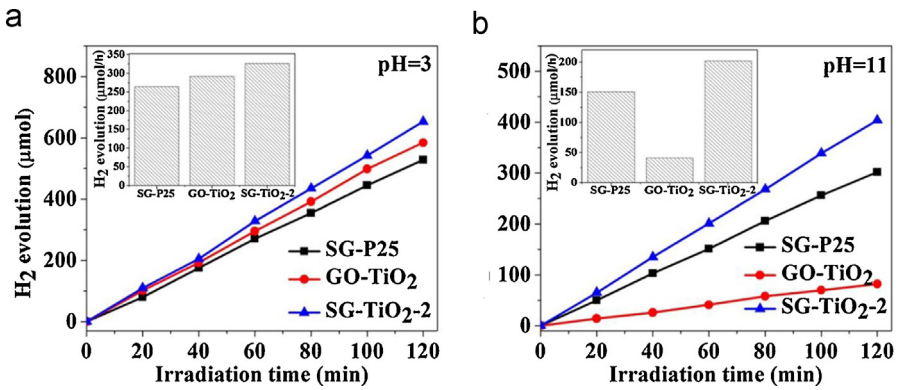

Fig. 10. Hydrogen production activity of SG–TiO_2-2, GO–TiO_2 (2 wt% of GO) and SG-P25 (2 wt% of SG) under pH = 3 (a) and pH = 11 (b) (inset: average hydrogen evolution rate).

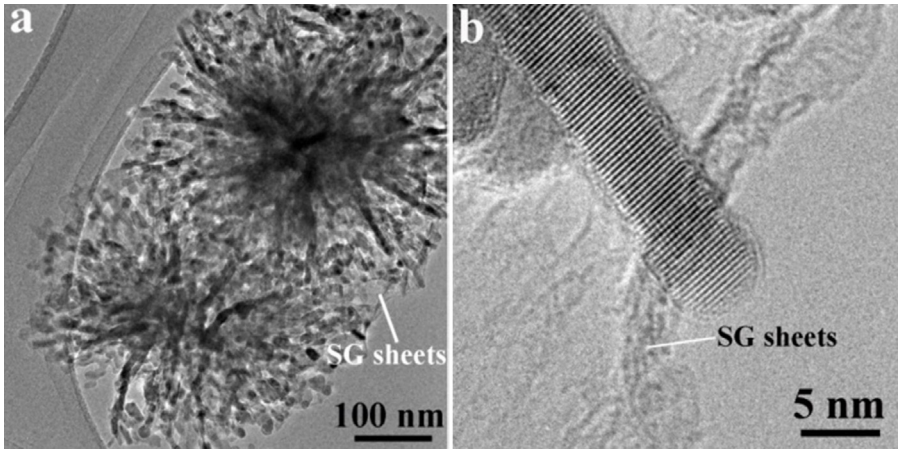

Fig. 11. TEM (a) and HRTEM (b) images of SG–TiO_2-2 after hydrogen production activity under pH = 11.

hydrogen generation rate under acidic condition (pH = 3) can be attributed to more H^+ ions existed in the solution. H^+ ions have more chance to be adsorbed on the surface of the photocatalysts and the reduction rate of H^+ to hydrogen by the photo-generated electrons will be increased [51]. Interestingly, a different phenomenon was observed when the photocatalysts worked under pH = 11 (basic condition). Fig. 10b shows that SG–TiO_2-2 and SG-P25 produce 404 μmol and 302 μmol of H_2 during 2 h, respectively. The average hydrogen evolution rates of SG–TiO_2-2 and SG-P25 are 202 μmol/h and 151 μmol/h under pH = 11, respectively, which are lower than that under pH = 7. This is because less H^+ ions can be reduced in the alkaline solution. Particularly, a distinctive curve of GO–TiO_2 was obtained under pH = 11, as seen in Fig. 10b. The hydrogen evolution rate of GO–TiO_2 is significantly reduced under pH = 11, and only 41 μmol of H_2 can be generated per hour, while GO–TiO_2 shows a greatly higher hydrogen evolution rate (ca. 245 μmol/h) under neutral pH. As shown in Fig. 7b, GO–TiO_2 exhibits better hydrogen production activity than SG-P25 under pH = 7. However, GO–TiO_2 shows the lowest hydrogen evolution rate (41 μmol/h) among three tested samples, even much lower than that of SG-P25, as seen in Fig. 9b. According to our knowledge, no one reported such discovery, so the reason behind this specific behavior was investigated in our experiments.

The morphology of SG–TiO_2-2 and GO–TiO_2 after hydrogen production under pH = 11 was characterized by TEM, as shown in Fig. 11 and S3. Fig. 11a shows the low magnification TEM image of SG–TiO_2-2. It can be clearly observed that SG sheets are connected with TiO_2 spheres after hydrogen production under pH = 11. HRTEM image (Fig. 11b) of SG–TiO_2-2 exhibits the characterized wrinkles of SG sheets and the clear lattice fringe of TiO_2 spheres. Fig. S3 are the TEM images of GO–TiO_2 after hydrogen generation under pH = 11. Several dispersed TiO_2 spheres can be seen in Fig. S3a. In addition, we cannot find the existence of GO sheets in Fig. S3a. Furthermore, one independent GO sheet can be observed in Fig. S3b, indicating that GO sheets cannot be grafted on the TiO_2 spheres under alkaline condition. The detaching of GO sheets from GO–TiO_2 composites is the main reason of the decrease of hydrogen evolution rate because the charge separation efficiency can be significantly reduced. In addition, the detached GO sheets can block the penetration and absorption of light, which further destroy the hydrogen production activity. The results indicate that the coordination bonds between the TiO_2 and the sulfonic group of SG sheets can tolerate a wide pH range, while the bonds between the TiO_2 and the carboxylic group of GO sheets can be damaged under basic condition. Hence, the SG–TiO_2 composites are suitable for the practical clean energy production.

4. Conclusion

In summary, SG–TiO_2 composites were successfully synthesized and well characterized by FESEM, TEM, XRD, FTIR, XPS, BET, UV–vis and PL. SG–TiO_2 composites with the optimal amount of SG sheets (2%) achieve a hydrogen evolution rate of 260 μmol/h, which is higher than standard P25 nanoparticles, pure TiO_2 spheres and GO–TiO_2 composites. The excellent hydrogen production activity of SG–TiO_2 composites can be attributed to large specific surface area, enhanced light absorption and efficient charge separation. More importantly, SG–TiO_2 composites show high hydrogen production

efficiency within a wide pH range (from pH = 3 to pH = 11), compared with GO–TiO_2 composites which loss photocatalytic activity dramatically under alkaline condition. This special property of SG–TiO_2 composites can be owed to the strong interaction between SG sheets and TiO_2 spheres. Hence, this study highlights that SG–TiO_2 composite can be a stable and efficient photocatalyst for clean energy production under various pH conditions.

Acknowledgements

Authors would like to acknowledge the Clean Energy Research Programme under National Research Foundation of Singapore for their research grant (Grant No. NRF2007EWT-CERP01-0420) support for this work. We would also like to thank CESEL and Facts for the use of AFM, FESEM and TEM.

Appendix A. Supplementary data

Supplementary data associated with this article can be found, in the online version, at http://dx.doi.org/10.1016/j.apcatb.2013.10.025.

References

[1] E. Chornet, S. Czernik, Nature 418 (2002) 928–929.
[2] X. Chen, L. Liu, P.Y. Yu, S.S. Mao, Science 331 (2011) 746–750.
[3] X. Chen, S. Shen, L. Guo, S.S. Mao, Chem. Rev. 110 (2010) 6503–6570.
[4] A. Fujishima, K. Honda, Nature 238 (1972) 37–38.
[5] A. Fujishima, X. Zhang, D.A. Tryk, Surf. Sci. Rep. 63 (2008) 515–582.
[6] X. Chen, S.S. Mao, Chem. Rev. 107 (2007) 2891–2959.
[7] C. Liu, X. Han, S. Xie, Q. Kuang, X. Wang, M. Jin, Z. Xie, L. Zheng, Chem. Asian J. 8 (2013) 282–289.
[8] L. Deng, S. Wang, D. Liu, B. Zhu, W. Huang, S. Wu, S. Zhang, Catal. Lett. 129 (2009) 513–518.
[9] J. Wang, D.N. Tafen, J.P. Lewis, Z.L. Hong, A. Manivannan, M.J. Zhi, M. Li, N.Q. Wu, J. Am. Chem. Soc. 131 (2009) 12290–12297.
[10] J. Yu, Q. Li, S. Liu, M. Jaroniec, Chem. Eur. J. 19 (2013) 2433–2441.
[11] Y. Gao, P. Fang, Z. Liu, F. Chen, Y. Liu, D. Wang, Y. Dai, Chem. Asian J. 8 (2013) 204–211.
[12] L.G. Devi, R. Kavitha, Appl. Catal., B 140–141 (2013) 559–587.
[13] L.X. Yang, S.L. Luo, Y. Li, Y. Xiao, Q. Kang, Q.Y. Cai, Environ. Sci. Technol. 44 (2010) 7641–7646.
[14] P. Gao, J. Liu, T. Zhang, D.D. Sun, W. Ng, J. Hazard. Mater. 229–230 (2012) 209–216.
[15] J. Xing, Z.P. Chen, F.Y. Xiao, X.Y. Ma, C.Z. Wen, Z. Li, H.G. Yang, Chem. Asian J. 8 (2013) 1265–1270.
[16] K. Woan, G. Pyrgiotakis, W. Sigmund, Adv. Mater. 21 (2009) 2233–2239.
[17] Q. Xiang, J. Yu, M. Jaroniec, J. Am. Chem. Soc. 134 (2012) 6575–6578.
[18] Q. Xiang, J. Yu, M. Jaroniec, Nanoscale 3 (2011) 3670–3678.
[19] P. Gao, Z. Liu, M. Tai, D.D. Sun, W. Ng, Appl. Catal., B 138–139 (2013) 17–25.
[20] J.H. Byeon, Y.W. Kim, ACS Appl. Mater. Interfaces 5 (2013) 3959–3966.
[21] W. Tu, Y. Zhou, Q. Liu, S. Yan, S. Bao, X. Wang, M. Xiao, Z. Zou, Adv. Funct. Mater. 23 (2013) 1743–1749.
[22] J. Zhang, Z. Zhu, Y. Tang, X. Feng, J. Mater. Chem. A 1 (2013) 3752–3756.
[23] S. Anandan, T. Narasinga Rao, M. Sathish, D. Rangappa, I. Honma, M. Miyauchi, ACS Appl. Mater. Interfaces 5 (2012) 207–212.
[24] A.A. Ismail, R.A. Geioushy, H. Bouzid, S.A. Al-Sayari, A. Al-Hajry, D.W. Bahnemann, Appl. Catal., B 129 (2013) 62–70.
[25] J. Wang, P. Wang, Y. Cao, J. Chen, W. Li, Y. Shao, Y. Zheng, D. Li, Appl. Catal., B 136–137 (2013) 94–102.
[26] P. Wang, J. Wang, X. Wang, H. Yu, J. Yu, M. Lei, Y. Wang, Appl. Catal., B 132–133 (2013) 452–459.
[27] S. Guo, S. Dong, Chem. Soc. Rev. 40 (2011) 2644–2672.
[28] S. Bai, X. Shen, RSC Adv. 2 (2012) 64–98.
[29] X. An, J.C. Yu, F. Wang, C. Li, Y. Li, Appl. Catal., B 129 (2013) 80–88.
[30] X.Y. Zhang, H.P. Li, X.L. Cui, Y. Lin, J. Mater. Chem. 20 (2010) 2801–2806.
[31] H.I. Kim, G.H. Moon, D. Monllor-Satoca, Y. Park, W. Choi, J. Phys. Chem. C 116 (2012) 1535–1543.
[32] P. Cheng, Z. Yang, H. Wang, W. Cheng, M. Chen, W. Shangguan, G. Ding, Int. J. Hydrogen Energy 37 (2012) 2224–2230.
[33] P. Gao, D.D. Sun, Chem. Asian J. (2013).
[34] J. Liu, H. Bai, Y. Wang, Z. Liu, X. Zhang, D.D. Sun, Adv. Funct. Mater. 20 (2010) 4175–4181.
[35] T. Zhang, J. Liu, D.D. Sun, RSC Adv. 2 (2012) 5134–5137.
[36] W.S. Hummers, R.E. Offeman, J. Am. Chem. Soc. 80 (1958), 1339-1339.
[37] P. Gao, J. Liu, S. Lee, T. Zhang, D.D. Sun, J. Mater. Chem. 22 (2012) 2292–2298.
[38] J. Liu, H. Jeong, K. Lee, J.Y. Park, Y.H. Ahn, S. Lee, Carbon 48 (2010) 2282–2289.
[39] P. Gao, J. Liu, D.D. Sun, W. Ng, J. Hazard. Mater. 250–251 (2013) 412–420.
[40] P. Gao, Z.Y. Liu, D.D. Sun, J. Mater. Chem. A (2013), in press.
[41] H.B. Wu, X.W. Lou, H.H. Hng, Chem. Eur. J. 18 (2012) 2094–2099.
[42] J.S. Chen, C. Chen, J. Liu, R. Xu, S.Z. Qiao, X.W. Lou, Chem. Commun. 47 (2011) 2631–2633.
[43] J.H. Pan, H. Dou, Z. Xiong, C. Xu, J. Ma, X.S. Zhao, J. Mater. Chem. 20 (2010) 4512–4528.
[44] Q. Li, B. Guo, J. Yu, J. Ran, B. Zhang, H. Yan, J.R. Gong, J. Am. Chem. Soc. 133 (2011) 10878–10884.
[45] Y. Xu, H. Bai, G. Lu, C. Li, G. Shi, J. Am. Chem. Soc. 130 (2008) 5856–5857.
[46] Y. Liu, R. Deng, Z. Wang, H. Liu, J. Mater. Chem. 22 (2012) 13619–13624.
[47] L. Zhang, J. Xia, Q. Zhao, L. Liu, Z. Zhang, Small 6 (2010) 537–544.
[48] J. Du, X. Lai, N. Yang, J. Zhai, D. Kisailus, F. Su, D. Wang, L. Jiang, ACS Nano 5 (2010) 590–596.
[49] B. Jiang, C. Tian, Q. Pan, Z. Jiang, J.Q. Wang, W. Yan, H. Fu, J. Phys. Chem. C 115 (2011) 23718–23725.
[50] P. Gao, M.H. Tai, D.D. Sun, ChemPlusChem (2013), in press.
[51] A.A. Nada, M.H. Barakat, H.A. Hamed, N.R. Mohamed, T.N. Veziroglu, Int. J. Hydrogen Energy 30 (2005) 687–691.